Available online at www.sciencedirect.com
SCIENCE DIRECT
ELSEVIER
Ocean Engineering 33 (2006) 1299–1321
OCEAN ENGINEERING
www.elsevier.com/locate/oceaneng

An experimental model application of wavescreen: Dynamic pressure, water particle velocity, and wave measurements

O. Yagci *, V.S.O. Kirca, M.S. Kabdasli, A.O. Celik, N.E. Unal, A. Aydingakko

Civil Engineering Faculty, Division of Hydraulics, Istanbul Technical University, 34469 Maslak, Istanbul, Turkey

Received 21 February 2005; accepted 11 August 2005
Available online 14 November 2005

Abstract

This paper analyses the results of an application of a piled wavescreen. Experimental measurements were undertaken in the laboratory conditions for a given structural configuration under the attack of regular and irregular waves. Dynamic pressure distribution along and around the inclined piles was obtained employing pressure transducers. Using these data, in-line dynamic wave forces acting on piles were also determined. Water particle (orbital) velocities were measured at seaward and landward of the wavescreen using two acoustic Doppler velocimeters (ADV) simultaneously. Furthermore, wave data were collected using resistance type wave gauges at the seaward and landward of the structure. Based on those data, wave attenuation performance of the wavescreen was explored for two different depth values. Findings showed that piled wavescreen can provide effective shore protection as an environmentally friendly coastal structure.

Keywords: Breakwater; Flume; Wave force; Inclined cylinder; Irregular wave; Pile, Dynamic pressure; Regular wave; Water particle; Wavescreen

* Corresponding author. Tel.: +90 212 285 6011; fax: +90 212 285 3418.
E-mail address: oyagci@ins.itu.edu.tr (O. Yagci).

0029-8018/$ - see front matter © 2005 Elsevier Ltd. All rights reserved.
doi:10.1016/j.oceaneng.2005.08.005

Nomenclature

ADV	acoustic Doppler velocimeters (–)
RMB	rubble mound breakwaters (–)
SWL	still water level (–)
d	depth (m)
D	pile diameter (m)
d*	reference depth (m)
f	freeboard (m)
f_x	distributed in-line dynamic wave force (kN/m)
g	gravitational acceleration (m/s^2)
H	wave height (m)
H_i	incident wave height (m)
H_{max}	maximum wave height (m)
H_{rms}	root mean square wave height (m)
H_s	significant wave height (m)
H_t	transmitted wave height (m)
L	wave length (m)
P	wave pressure (kN/m^2)
P_d	dynamic wave pressure (kN/m^2)
P_{dX}	in-line component of dynamic wave pressure (kN/m^2)
P_d^*	reference dynamic wave pressure (kN/m^2)
S	spacing between the piles (m)
T	wave period (s)
T_{mean}	mean wave period (s)
u, v, w	three components of water particle velocity (m/s)
α	vertical inclination angle of piles (degree)
θ	angle on the horizontal plane (radian)
θ_r	angles between transducers and incident wave direction (degree)

1. Introduction

Various shore protection techniques and structures have been developed and applied to minimize the wave impact on coastal areas. Rubble mound breakwaters are one of the most commonly utilized coastal structures in shore protection facilities. In certain circumstances, it may not be possible to apply rubble mound breakwaters (RMB) in shore protection due to some technical, economical and environmental limitations. In such cases, although not preferred as much as RMB, piled breakwaters may be used as an alternative. There are particular applications, where piled breakwaters are preferable over RMB. For example, when foundation instability is high, the uncertainty in behavior of armor layer of RMB increases in the long term. Furthermore, piled breakwaters do not

totally cut the current or wave action and do not entirely stop the sediment transport phenomenon. These factors make piled breakwaters environmentally friendly, as they keep the long-term coastal balance better then RMB. In fact, it may be more appropriate to call such a piled structure as 'wavescreen'; since it acts as a screen against waves and decreases the wave effect, but does not entirely stop the wave activity by transmitting just a certain ratio of the wave energy.

Offshore and marine structures are designed considering maximum wave loads that may appear during their lifetime. In this context, determination of the wave forces which will act on the piles under the storm condition is a vital issue for a wavescreen. For a fixed vertical cylinder, whose diameter is small enough compared to the wavelength, the total force is composed of two components. These components are 'inertia' and 'drag' terms. Total force can be computed by Morison's equation (Morison et al., 1950). In the literature, great efforts have been devoted to investigating the drag (C_D) and inertia (C_M) coefficients in Morison's equation (Garrison et al., 1977; Chakrabarti, 1982; Chakrabarti et al., 1983; Cotter and Chakrabarti, 1984). According to Akyildiz (2002), there are basically two different approaches for evaluating the non-linear hydrodynamic wave forces acting on an offshore structure: 'Morison's equation' and 'diffraction flow theory'. Sumer and Fredsoe (1997) pointed out that the ratio between diameter, D, of the cylinder and wave length, L, provides the required information on which theory should be used. If D/L ratio is greater than 0.2, the diffraction effect is important and if this ratio is lower than 0.2 the diffraction effect can be disregarded. Another important geometrical variable is the inclination angle of the cylinders. Anandkumar et al. (1995) experimentally investigated pressures around circular inclined cylinder under regular waves. Later on, Sundar et al. (1998) presented the variation of C_D and C_M coefficients as a function of Keulegan–Carpenter number (KC) for different inclination of the cylinder. This is followed by Sundar et al. (1999), who investigated dynamic pressure distribution around an inclined cylinder under freak waves ($H_{max}/H_{1/3} > 2.0$). In the literature there are fewer studies on multiple-cylinders compared with singular ones. The studies pertain to Sarpkaya (1976), Chakrabarti (1978, 1981), and Sarpkaya (1979) may be given as reference studies focused on this issue. Further, Chan et al. (1995) conducted an experimental study and explored the plunging wave impact on vertical cylinders.

Based on the arguments presented above, a laboratory study was performed and a set of experimental measurements was carried out for a particular wavescreen. The primary objectives of those experiments may be summarized as:

(1) to measure the in-line dynamic pressure distribution along the piles tilted along the principal wave direction,
(2) to measure the dynamic pressure distribution around the piles,
(3) to determine the wave forces acting on the inclined piles using measured dynamic wave pressures,
(4) to define the performance of the wavescreen in terms of the wave attenuation; in other words exploring wave transmission coefficient for various wave conditions,
(5) to monitor the orbital velocity pattern for different depth and wave conditions.

2. Experiments

2.1. Experimental installation and measurement devices

All the experiments described in this paper were conducted in the Hydraulics Laboratory of Istanbul Technical University. The experiments were performed under the attack of regular and irregular waves in a glass sided wave flume 24 m in length, 1 m in width, and 1 m in depth. The sketch of the flume and locations of the measurement devices are illustrated in Fig. 1. The waves were generated by a computer controlled wave maker, which is capable of generating regular waves as well as irregular waves displaying the Pierson–Moskowitz wave spectrum. Further details about the performance of the irregular wave flume utilized in this study may be found in Yagci et al. (2004). The tests were carried out for 0.65 and 0.75 m still water depth values. At landward of the wavescreen, a sand beach slope, 1V:7H, was constructed at the end of the channel as a wave dissipater (Fig. 1).

The wavescreen model was made of plexiglas material in view of the ease of construction and placement of the waterproof pressure measurement probes. In order to place the transducers into the piles, the angled piles on the model structure were also made of plexiglas. Furthermore, the transparency of the plexiglas makes it an ideal material for such studies to facilitate better visualization. The heading beam was represented as a box of plexiglas. The sketch and dimensions of the wavescreen are presented in Fig. 2.

For the measurement of dynamic wave pressures acting on the piles, seven pressure transducers were used throughout the experiments. The locations of the transducers along the piles are also presented in Fig. 2. So as to measure the pressure distribution around the cylinder, the system was designed to allow rotation of the cylinder around its axis. The same wave condition was repeated (Table 1) for each rotation angle of the cylinder (i.e. 0, 22.5, 45, 67.5, 90°). The transducers were connected to computer via a data-logger which

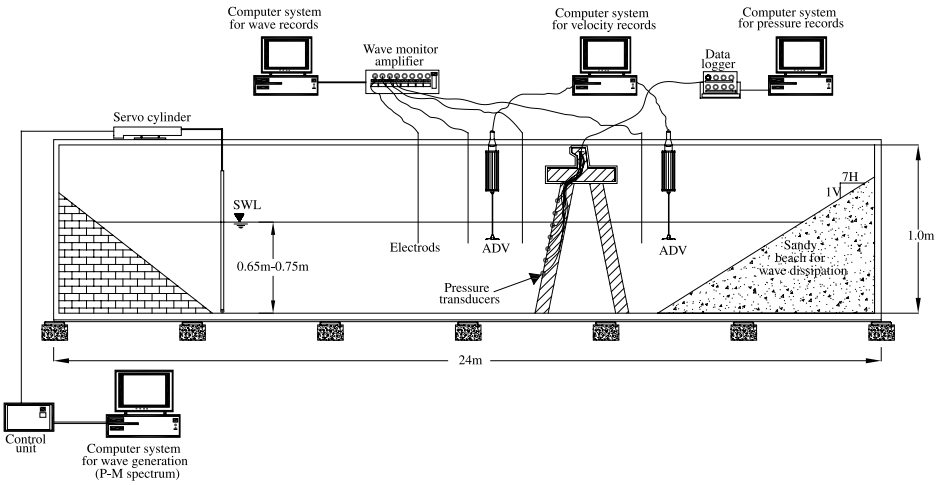

Fig. 1. Sketch of the wave flume.

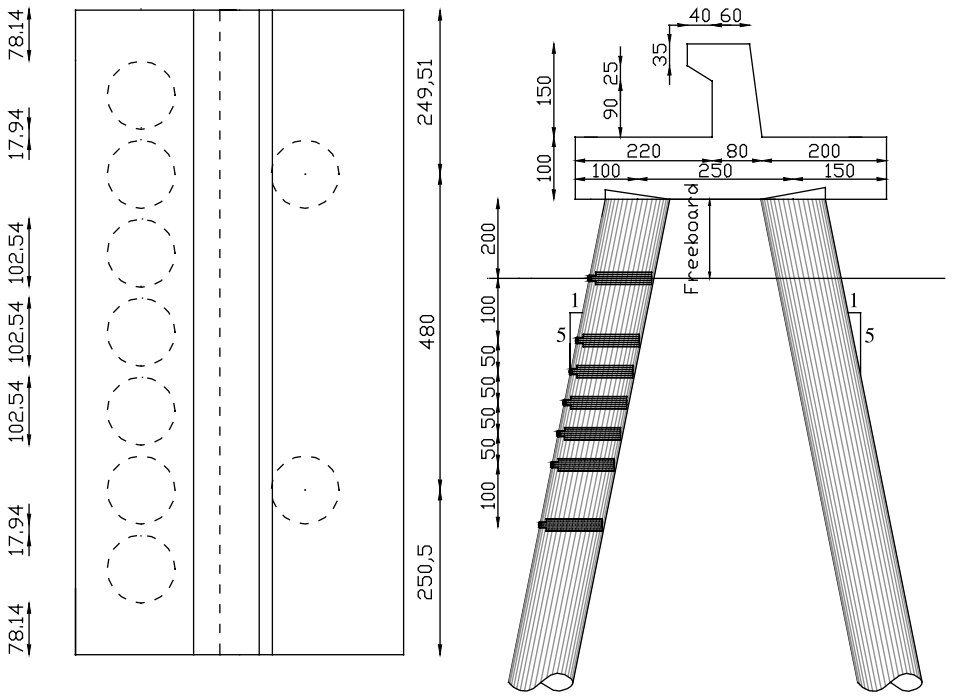

Fig. 2. (a) Plan and (b) side sketch of the model wavescreen (in mm).

has 16 channels. The sampling frequency of pressure data acquisition was 20 Hz throughout the experiments. The calibration of the transducers was done by the manufacturer.

A wave monitor amplifier and four resistance type wave electrodes were employed throughout the measurements of the wave records. The locations of the wave probes are depicted in Fig. 1. The wave data were collected with a sampling frequency of 20 Hz. The digital signals were converted to wave height, and wave period parameters by a program written in Borland C 2.0 language by Istanbul Technical University, Division of Hydraulics. In this code, time series parameters were determined using a zero-downcrossing method. The analysis and the statistics of the recorded wave data were also computed by the same Borland C 2.0 code after each applied wave series. At the end of each series, the calibration process was repeated.

So as to understand how the wavescreen impacts the water particle velocities of a progressive regular wave, two acoustic doppler velocimeters (ADV), which have 25 Hz sampling frequency, were utilized. Usage of two ADV simultaneously allows collecting orbital velocity data more reliably compared to collecting data with a single ADV and also it is time saving. The ADV is a high precision instrument that measures all three flow velocity components. ADV consists of three modules: the measuring probe, the conditioning module and processing module. The acoustic sensor of the 3D down-looking

Table 1
Experimental schedule

Test no.	Still water depth (m)	Applied wave characteristics		Velocity measurements with ADV		Pressure measurements around the piles		Pressure measurements along the piles
		Name of the wave series	Reg./ Irreg.	Yes/No	Distance from channel bottom	Yes/No	Angle	Yes/No
1	0.65	23	Reg.	Yes	0.03	Yes	0	Yes
2	0.65	23	Reg.	Yes	0.06	Yes	22.5	No
3	0.65	23	Reg.	Yes	0.09	Yes	45.0	No
4	0.65	23	Reg.	Yes	0.12	Yes	67.5	No
5	0.65	23	Reg.	Yes	0.15	Yes	90.0	No
6	0.65	23	Reg.	Yes	0.20	No	–	No
7	0.65	23	Reg.	Yes	0.25	No	–	No
8	0.65	23	Reg.	Yes	0.30	No	–	No
9	0.65	23	Reg.	Yes	0.35	No	–	No
10	0.65	23	Reg.	Yes	0.40	No	–	No
11	0.65	23	Reg.	Yes	0.45	No	–	No
12	0.65	13	Reg.	No	–	No	–	Yes
13	0.65	31	Reg.	No	–	No	–	Yes
14	0.65	51	Reg.	No	–	No	–	Yes
15	0.65	1	Irreg.	No	–	No	–	Yes
16	0.65	2	Irreg.	No	–	No	–	Yes
17	0.65	3	Irreg.	No	–	No	–	Yes
18	0.65	4	Irreg.	No	–	No	–	Yes
19	0.65	5	Irreg.	No	–	No	–	Yes
20	0.65	6	Irreg.	No	–	No	–	Yes
21	0.65	7	Irreg.	No	–	No	–	Yes
22	0.75	23	Reg.	Yes	0.03	Yes	0	Yes
23	0.75	23	Reg.	Yes	0.06	Yes	22.5	No
24	0.75	23	Reg.	Yes	0.09	Yes	45.0	No
25	0.75	23	Reg.	Yes	0.12	Yes	67.5	No
26	0.75	23	Reg.	Yes	0.15	Yes	90.0	No
27	0.75	23	Reg.	Yes	0.20	No	–	No
28	0.75	23	Reg.	Yes	0.25	No	–	No
29	0.75	23	Reg.	Yes	0.30	No	–	No
30	0.75	23	Reg.	Yes	0.35	No	–	No
31	0.75	23	Reg.	Yes	0.40	No	–	No
32	0.75	23	Reg.	Yes	0.45	No	–	No
33	0.75	23	Reg.	Yes	0.50	No	–	No
34	0.75	23	Reg.	Yes	0.55	No	–	No
35	0.75	13	Reg.	No	–	No	–	Yes
36	0.75	31	Reg.	No	–	No	–	Yes
37	0.75	51	Reg.	No	–	No	–	Yes
38	0.75	1	Irreg.	No	–	No	–	Yes
39	0.75	2	Irreg.	No	–	No	–	Yes
40	0.75	3	Irreg.	No	–	No	–	Yes
41	0.75	4	Irreg.	No	–	No	–	Yes
42	0.75	5	Irreg.	No	–	No	–	Yes
43	0.75	6	Irreg.	No	–	No	–	Yes
44	0.75	7	Irreg.	No	–	No	–	Yes

probe is mounted on a rigid stem 0.4 m long and is composed of one transmit transducer and three receive transducers. ADV measures the velocity in a sampling volume of 0.125 cm^3 which is 5 cm away from the sensing elements. The ADV processing module consisted of a PC card, installed in a PC, and data acquisition software. Two velocity components (u and w) of the orbitals along the depth were obtained with sampling durations of 30 s for each test. During the measurements one ADV was positioned at seaward and the other one at landward of the wavescreen (Fig.1). Moreover, the distances between seaward ADV and wavescreen; landward ADV and wavescreen, were equal to each other.

2.2. Experimental procedure

The principal goals of the study are as summarized in the introduction section. In order to achieve these objectives, the experimental procedure, which is presented in Table 1, was adopted.

As may be seen from Table 1, all the experiments were performed for the depth values of 0.65 and 0.75 m. For each depth value, four regular and seven irregular wave series were applied to the structure. The test runs conducted with regular waves were limited to 30 s to minimize build up of reflected wave energy in the flume. While regular wave series had an application duration of 30 s, each irregular wave series had application duration of 8 min. For the tests conducted with regular waves, the ranges of wave period (T) and wave height (H) were 0.857–2.056 s and 0.112–0.185 m, respectively. In the tests carried out with irregular waves, the ranges of the mean wave period (T_{mean}), significant wave height (H_s), root mean square wave height (H_{rms}) and maximum wave height (H_{max}) were 1.146–1.502 s, 0.093–0.164 m, 0.065–0.121 m and 0.156–0.233 m, respectively. If sea conditions were not simulated properly in the laboratory, the obtained results would be misleading. Considering this point, so as to verify the validity of the experimental wave data, ratios between measured and analyzed wave height statistics were checked with the ratios between wave height statistics derived from Rayleigh distribution. These ratios are given by Goda (1985) and Dean and Dalrymple (1991). Ratios between those wave height statistics showed that the generated waves in the flume fitted Rayleigh distribution properly.

The measurements which aim to explore the pressure distribution along the inclined piles were carried out under regular and irregular waves. In order to characterize the recorded pressure values, the mean of the highest 30 pressure measurement values were taken as a representative value for each transducer. This value corresponds to $P_{1/3}$ for regular wave series and to $P_{1/20}$ for the irregular wave series.

As stated above, to measure the pressure distribution around the cylinder, the system was designed to allow rotation of the cylinder around its axis. Same regular wave condition (which is indicated with series no 23 in Table 1) was applied to the structure for each rotation angle of the pressure transducer (i.e. 0, 22.5, 45, 67.5, 90°).

In addition to dynamic in-line pressure measurements, dynamic in-line wave force distribution was also obtained for a specific wave series (referred to as series 23, see Table 1). This was simply done by multiplying the dynamic wave pressure values (P_d) measured around the cylinders with *cosine* of the inclination angles of the transducers

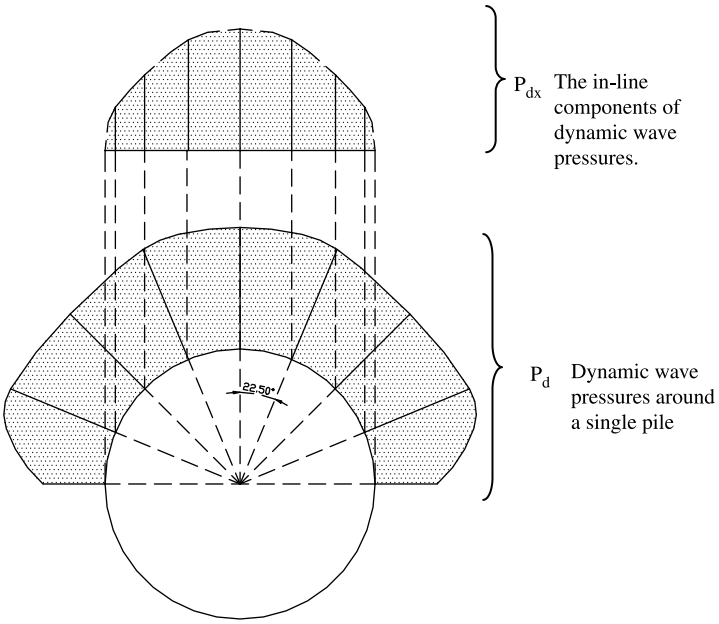

Fig. 3. Horizontal dynamic wave pressure distribution and in-line component of dynamic wave pressure on the pile.

from the normal axis ($\cos\theta_r$) (1) and then summing the in-line components of pressure values around the cylinder (2) (Fig. 3)

$$P_{dX} = \cos\theta_r P_d \tag{1}$$

$$f_x(y)dy = \int_{-\pi/2}^{\pi/2} P_{dX}(\theta)d\theta \tag{2}$$

The summation of the in-line components of dynamic wave pressures were made on a trapezoidal rule basis (Fig. 4). The vertically distributed in-line force along the cylinders ($f_x(y)dy$) was then determined for two different water depths as given in Section 3.

In order to compare all the measured dynamic in-line pressure data on the same basis it was necessary to use dimensionless values. Also the contribution of different wave parameters on the in-line dynamic wave pressures can be understood by defining convenient dimensionless parameters. A dimensionless parameter for dynamic pressure and three different dimensionless parameters for depth are defined and used for this objective as explained in Section 3.

In order to explore how water particle velocities are affected by presence of the wavescreen, the velocity measurements were carried out under a regular wave series at two different depths, i.e. 0.65 and 0.75 m (Table 1). As may be judged from Table 1, velocity measurements were performed at consecutive points with 0.03 m increments starting from the bottom to a distance of 0.15 m; this increment was then increased to be

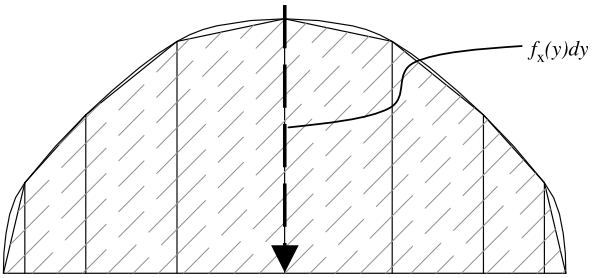

Fig. 4. The summation of distributed in-line pressure considering trapezoids: shaded region = $f(y)$dy.

0.05 m and the velocity measurements were carried out for each successive 0.05 m interval between depth values of 0.15 and 0.55 m (or 0.45 m for SWL = 0.65 m). Since ADV can collect data as long as it contacts with water, the elevation of the highest point, from which data can be collected, is limited by the elevation of wave trough. This situation is depicted in Fig. 5. The data acquisition duration was limited to 30 s for velocity measurements. Three components of the water particle velocities were obtained for each elevation after each test. In Fig. 6, measured three velocity components at 0.4 m distance from the bottom of the flume are given as a sample data. After obtaining three velocity components (u, v, and w) for each elevation, horizontal orbital velocity profiles along the depth were acquired using 'u'. Those results are presented and discussed in Section 3.

Wave transmission is an important parameter for the performance of permeable coastal protection structures. In order to define the wave damping performance of the structure, a parameter called wave transmission coefficient was defined as the transmitted wave height over incident wave height

$$C_t = H_t/H_i \tag{3}$$

where H_i, incident wave; H_t, transmitted wave. For the calculation of wave transmission coefficient the regular test results were employed. The experimental results are given in Section 3.

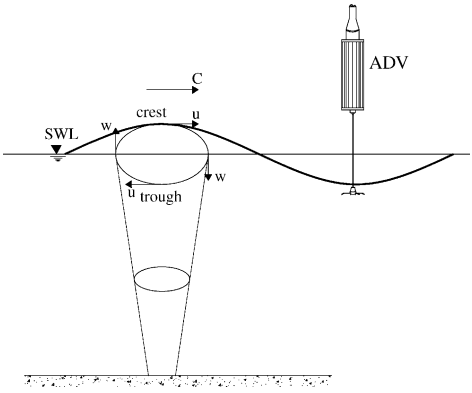

Fig. 5. Orbits of water particles in a wave cycles.

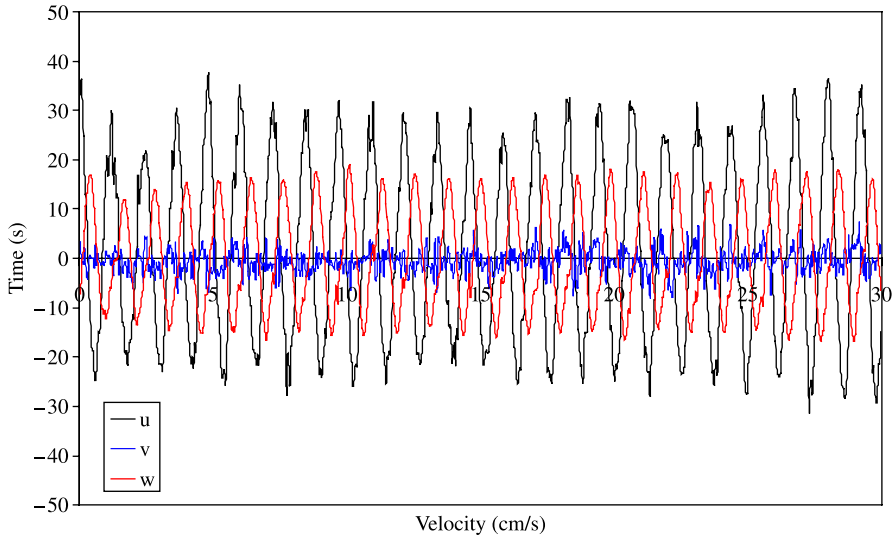

Fig. 6. Orbital velocities of water particles of incident waves measured at 40 cm from the bottom (SWL = 0.65 m).

3. Results

3.1. In-line dynamic wave pressures on the piles

All the pressure measurements made along the piles, with regard to test runs noted in Table 1, are presented in Fig. 7. In Fig. 7a, the vertical distribution of in-line dynamic wave pressures under regular wave series is given. The vertical distribution of in-line dynamic wave pressures under irregular wave series are given in two separate figures: in Fig. 7b the still water depth in the laboratory flume is 0.65 m and in Fig. 7c it is 0.75 m.

It was seen that there is not a simple proportional relation between wave height or wave period and in-line dynamic wave pressures on wavescreen. But the exponentially decaying character of pressures with depth can clearly be seen from the related figures. Also the logarithmic curves fitted to the pressure values gave good correlations (for regular waves, $R^2 = 0.74$–0.99 and for irregular waves $R^2 = 0.70$–0.98) which supports the previous values. On the other hand, it is obvious that such best fitting logarithmic curves never intersect $d = 0$ line; which means that they yield infinity pressure value at the still water level. Thus, it can be said that the correlation between actual P_d vs. d curve and best fitting logarithmic trend line weakens with d values approaching '0'. This statement also explains why the R^2 values of 0.75 m water level tests are higher than 0.65 m ones.

The same pressure measurements were also given in dimensionless form. For such a conversion, to define a reference depth 'd^*' and a reference pressure 'P_d^*' would be appropriate. Logically, the reference pressure would coincide with the reference depth (i.e. occurring at the reference depth). Considering the exponential nature of the P_d vs. d relationship, it is more reliable to define this reference depth (and thus the reference

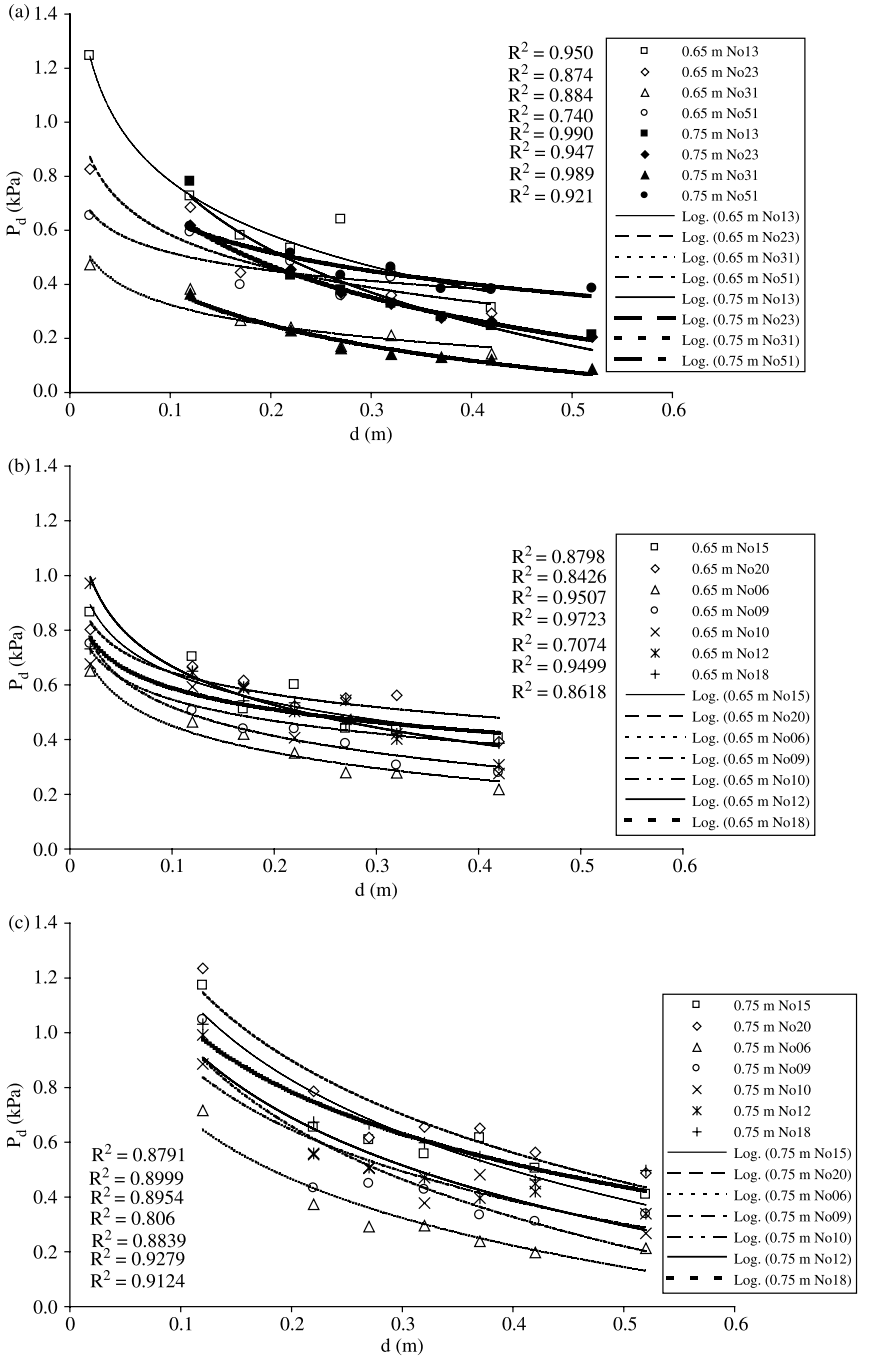

Fig. 7. In-line dynamic wave pressures (P_d) vs. distance from SWL (d); (a) under regular waves, (b) under irregular waves for SWL = 0.65 m, (c) under irregular waves for SWL = 0.75 m.

pressure) as deep as possible. Among all the transducers, the deepest pressure transducer was placed 0.42 m below SWL = 0.65 m. This value becomes 0.52 m for 0.75 m SWL. In order to compare both groups of tests (performed with two different SWLs), an additional pressure value was generated for each test carried out with 0.65 m SWL, which corresponds to 0.52 m depth due to the best fitting logarithmic curve (simply on the curve). Consequently, the reference depth 'd^*' was chosen as 0.52 m from the still water level.

Firstly, the dimensionless depth parameter was chosen as d/d^*, namely depth from SWL over reference depth, and the dimensionless pressure parameter was chosen as P_d/P_d^*, namely measured pressure over reference pressure. Such a dimensionless expression of the 'pressure vs. depth' is given in Fig. 8 for regular waves, irregular waves at 0.65 m SWL and irregular waves at 0.75 m SWL.

Another dimensionless parameter was generated in order to see the effect of wave height (H) on in-line dynamic wave pressures. Using a similar analogy with the normalization of standard normal variable, a combined dimensionless parameter defined as $(d-d^*)/H$ was calculated and plotted versus dimensionless in-line dynamic wave pressure. Fig. 9 shows these charts for regular waves, irregular waves at 0.65 m SWL and irregular waves at 0.75 m SWL. It would be convenient to note that the wave height (H) parameter was chosen as significant wave height (H_s) for irregular wave series.

As a final dimensionless parameter, the wave period (T) was also included in a dimensionless term that was chosen as $(d-d^*)/gT^2$. The same three plots are repeated for this parameter and given in Fig. 10 for regular waves, irregular waves at 0.65 m SWL and irregular waves at 0.75 m SWL. The mean period, 'T_{mean}', was chosen as representative wave period value for irregular waves.

In order to compare the scattering of dimensionless pressure values with the two different dimensionless parameters which represent wave height and wave period, two unique charts covering all tests are illustrated for both. These combined plots for P_d/P_d^* vs. $(d-d^*)/H$ and P_d/P_d^* vs. $(d-d^*)/gT^2$ were given in Figs. 11 and 12, respectively.

3.2. Dynamic wave pressures around the piles

The dynamic wave pressures around the piles were measured with 22.5° intervals for one regular wave series, no. 23, as explained in Section 2.2. The measurements were conducted for both at 0.65 and 0.75 m SWLs and dynamic wave pressure distribution around the piles was obtained. Figs. 13 and 14 present the dynamic wave pressure around the pile (referring to Fig. 3) at 0.65 and 0.75 m SWL, respectively.

The findings show that the maximum dynamic wave pressure does not always occur at the section normal to the wave direction. In other words, this infinitesimal surface may rotate and make an angle with the incident wave direction. For example, in Fig. 13 the maximum dynamic wave pressure around the pile can be seen to be closer to a location making an angle of 22.5° with the wave direction. This behavior may be explained by the multi-cylinder effect and possibly related to different parameters such as pile spacing, wave length, etc. In Fig. 14 the maximum dynamic pressures seem to occur at the differential surface element coinciding with the incident wave, but it cannot be said that dynamic wave pressure is decreasing with the angle with the wave direction.

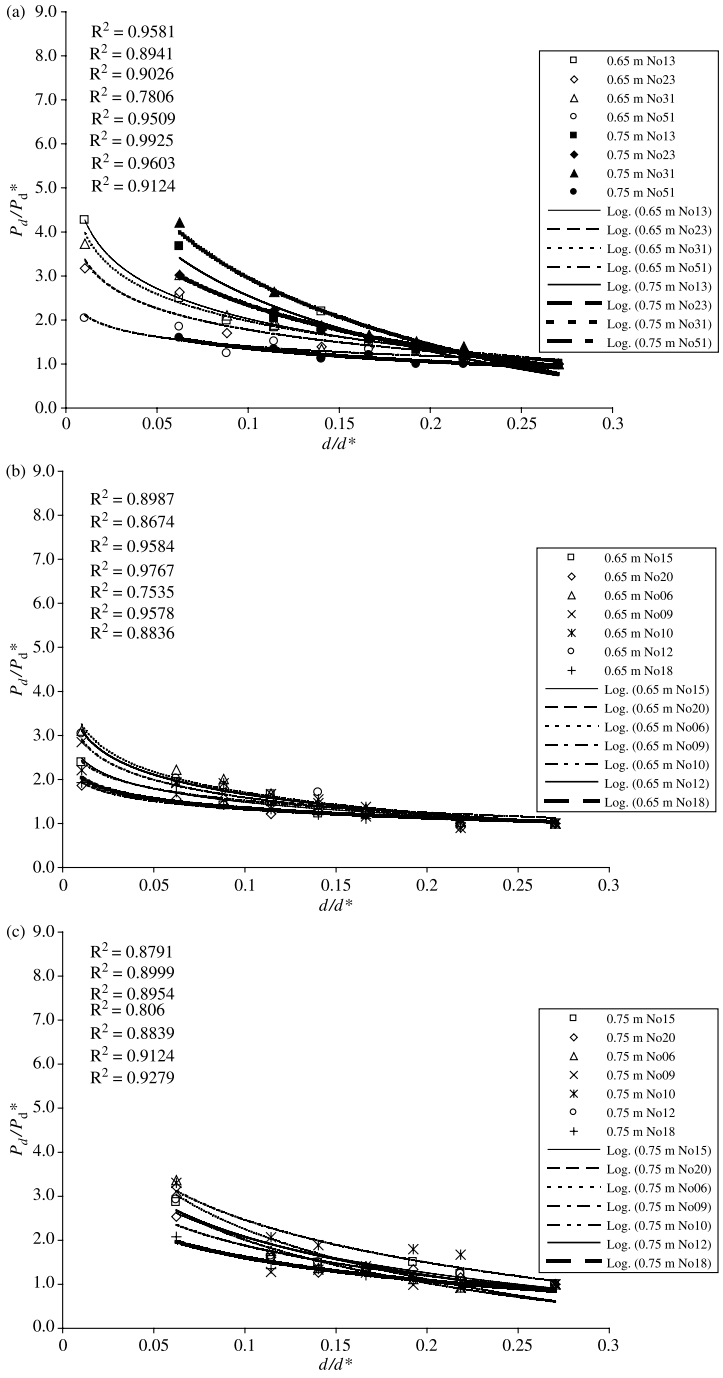

Fig. 8. In-line dimensionless dynamic wave pressure (P_d/P_d^*) vs. dimensionless depth (d/d^*): (a) under regular waves, (b) under irregular waves at SWL = 0.65 m, (c) under irregular waves at SWL = 0.75 m.

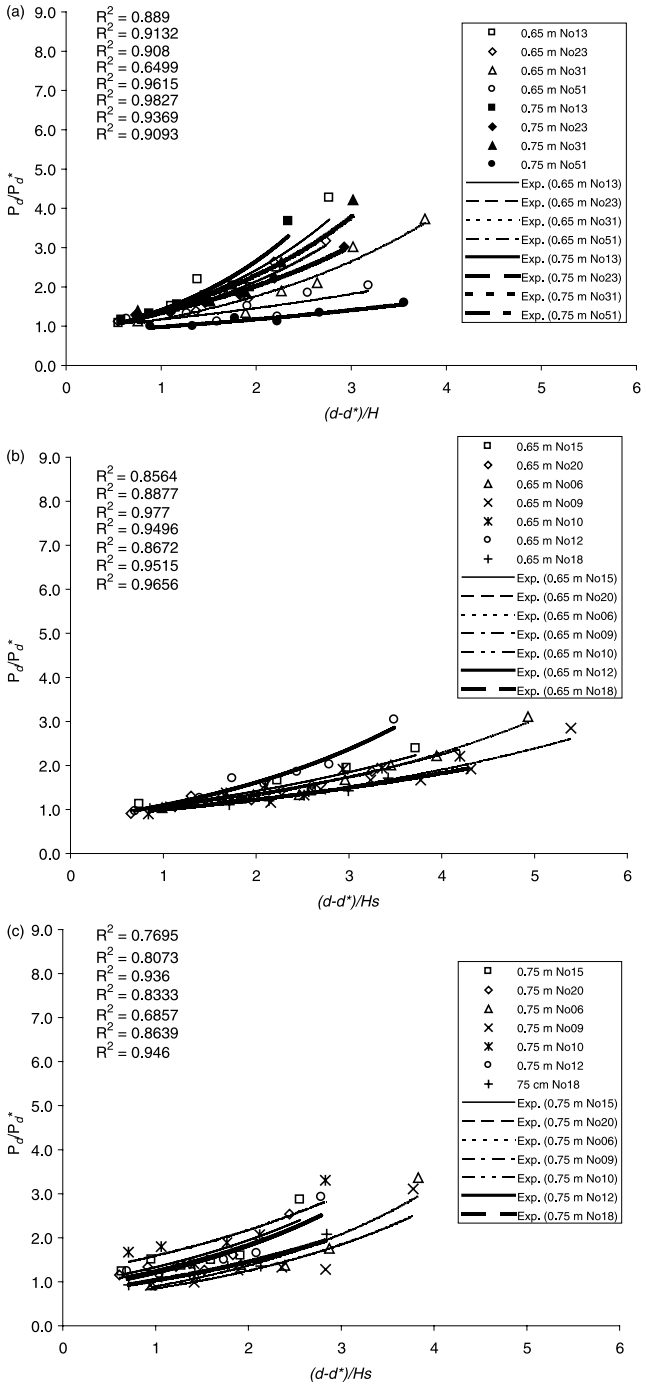

Fig. 9. In-line dimensionless dynamic wave pressure (P_d/P_d^*) vs. dimensionless depth-wave height ($(d-d^*)/H$): (a) under regular waves, (b) under irregular waves for SWL = 0.65 m, (c) under irregular waves for SWL = 0.75 m.

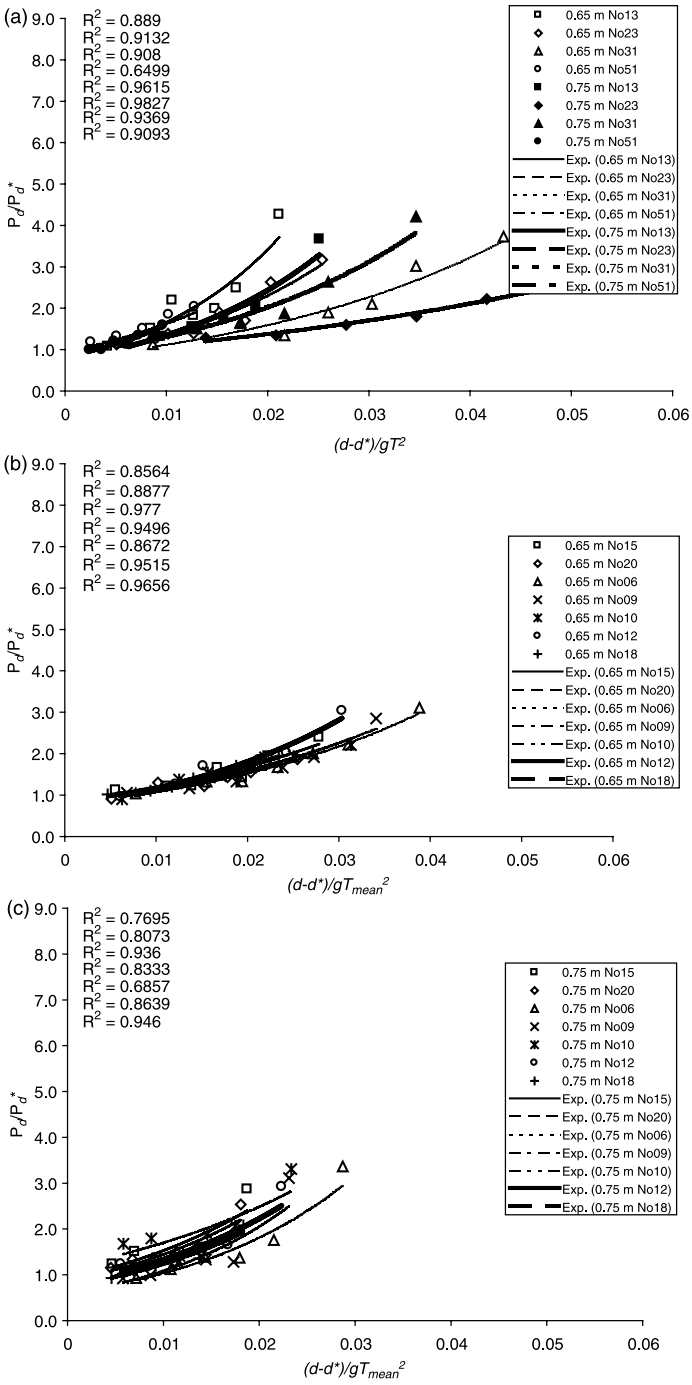

Fig. 10. In-line dimensionless dynamic wave pressure (P_d/P_d^*) vs. dimensionless depth-wave period ($(d-d^*)/gT^2$): (a) under regular waves, (b) under irregular waves for SWL = 0.65 m, (c) under irregular waves for SWL = 0.75 m.

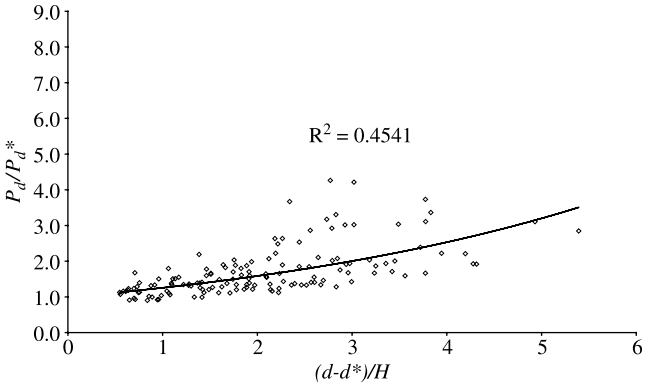

Fig. 11. In-line dimensionless dynamic wave pressure (P_d/P_d^*) vs. dimensionless depth-wave height ($(d-d^*)/H$).

3.3. In-line dynamic wave forces on the piles

The in-line dynamic wave force distribution on the piles was calculated for one regular wave series, no. 23, with a procedure explained in Section 2.2. This procedure was applied both at 0.65 and 0.75 m SWLs and vertical dynamic wave force distribution on the piles was obtained.

As a first step, the in-line components of dynamic wave pressures were obtained for the regular wave series, no. 23 (Table 1), at 0.65 and 0.75 m SWLs as given in Figs. 15 and 16, respectively.

By summing these in-line dynamic wave pressure components, dynamic in-line vertical wave force distributions for the regular wave were evaluated for 0.65 and 0.75 m SWLs as shown in Fig. 17. Similar to in-line dynamic wave pressures, also in-line dynamic wave force shows an exponential decay with depth.

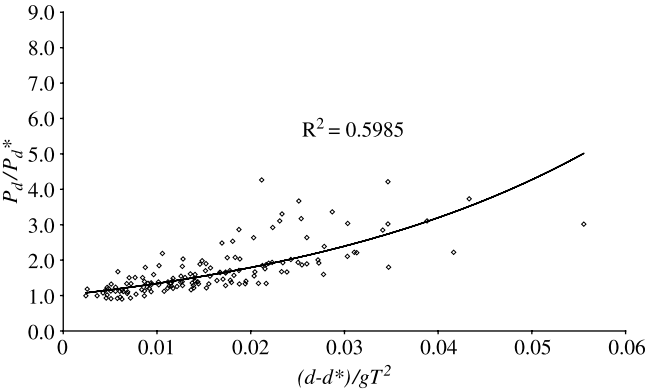

Fig. 12. In-line dimensionless dynamic wave pressure (P_d/P_d^*) vs. dimensionless depth-wave period ($(d-d^*)/gT^2$).

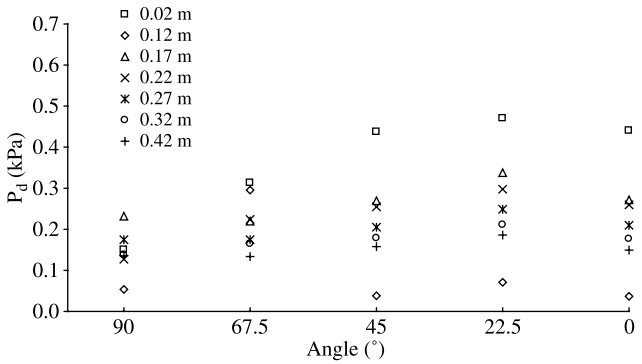

Fig. 13. Dynamic wave pressure values around the piles with respect to angles with the incident wave direction (regular wave, SWL = 0.65 m).

3.4. Measurements of water particle velocities

The experimental set up and the followed procedure for the water particle velocity measurements are as described in Sections 2.1 and 2.2, respectively. The notations for the water particle velocities are given in Fig. 5. In Fig. 18 three components of the water particle velocities which were measured at the seaward and landward are presented. The measurements presented in Fig. 18 were carried out at 0.45 m distance from the bottom for the SWL 0.65 m. In order to give the time series in a more intelligible way, only the data collected between 10 and 20 s time intervals are given in Fig. 18, though the measurement duration was 30 s. Despite the fact that similar measurements were conducted along the depth both at the landward and at the seaward as explained in Section 2.2; considering the limits of this paper, only the measurements recorded at 0.45 m distance from the bottom are given and analyzed here. As may be judged from Fig. 18, the particle velocity component '*u*' is much more affected compared to '*w*' by the presence of the wavescreen. Another conclusion, which can be drawn from Fig. 18, is about the variation of lateral

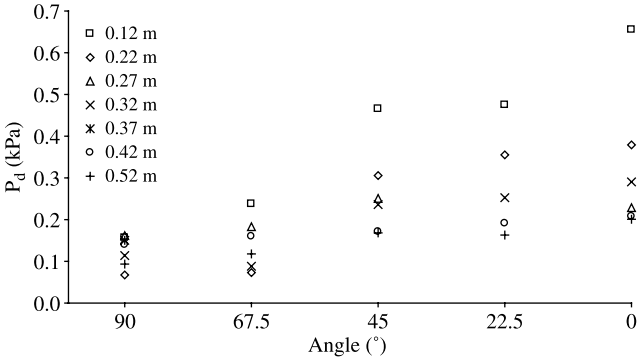

Fig. 14. Dynamic wave pressure values around the piles with respect to angles with the incident wave direction (regular wave, SWL = 0.75 m).

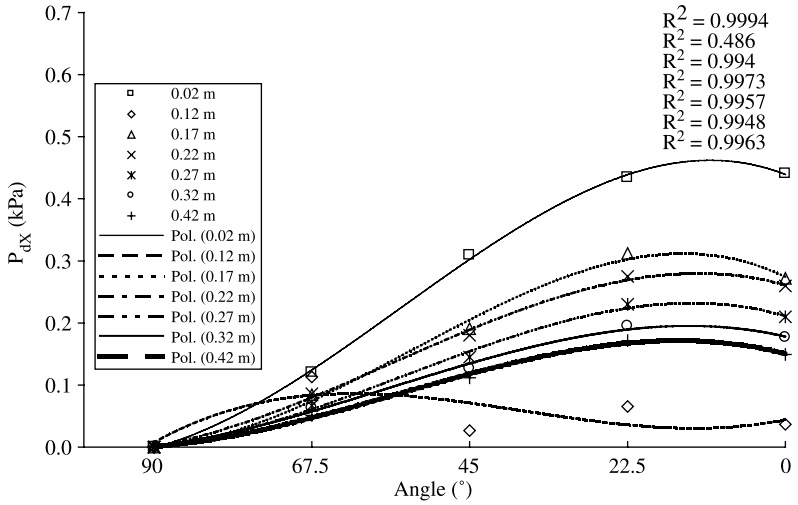

Fig. 15. In-line components of dynamic wave pressure values around the piles with respect to angles with the incident wave direction (regular wave, SWL = 0.65 m).

(spanwise) velocity component '*v*'. Based on Fig. 18, it may be claimed that a lateral momentum transfer occurs at the landward of the wavescreen which indicates additional minor energy dissipation.

The velocity profiles were obtained by following the method described in Section 2.2. The variation of velocity profiles with depth is illustrated in Fig. 19 for the conditions SWL = 0.65 and 0.75 m. The horizontal orbital velocity profiles along the depth were

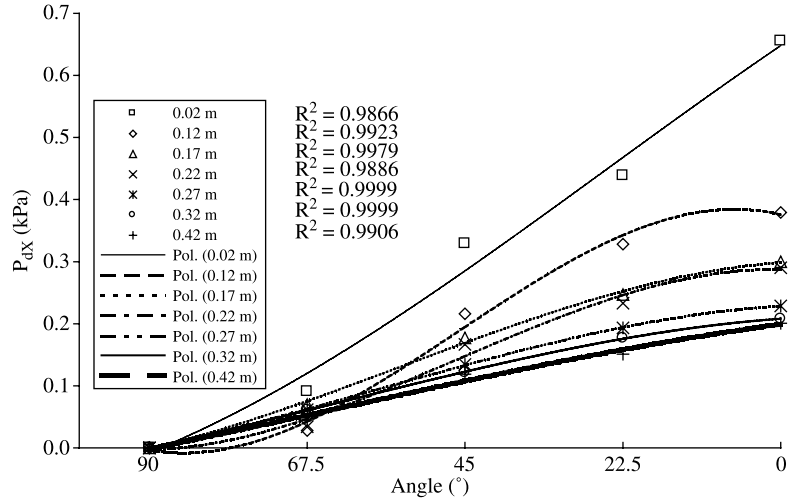

Fig. 16. In-line components of dynamic wave pressure values around the piles with respect to angles with the incident wave direction (regular wave, SWL = 0.75 m).

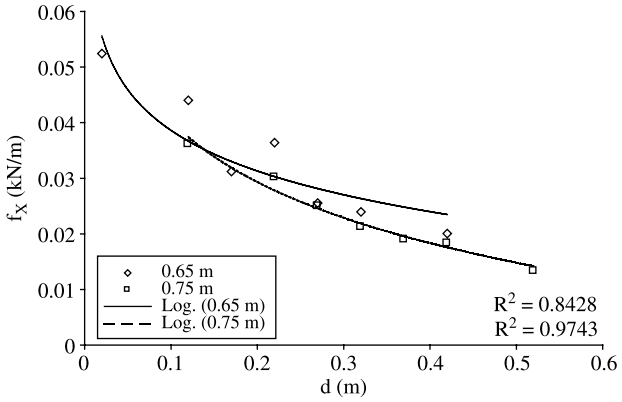

Fig. 17. Vertical dynamic wave force distribution on the piles (regular wave, SWL = 0.65 and 0.75 m).

obtained at the landward and seaward of the wavescreen. As may be concluded from Fig. 19, the wavescreen has greater impact in terms of wave attenuation within the region closer to the surface. On the other hand, in the region closer to the bottom, velocity values at the seaward and at the landward are quite close to each other for both SWL = 0.65 and 0.75 m. This result is important since it shows that wavescreen does not stop sediment transport though it dampens wave energy efficiently. In other words, wavescreen keeps the long-term coastal balance better then rubble mound breakwaters and this makes wavescreen an environmentally friendly structure.

3.5. Wave attenuation

The transmitted wave heights were evaluated by the data recorded from the wave probe behind the model structure at the 30 s duration regular tests. It was seen that C_t varies mostly due to the water level, such that at low water level it is higher and as the water level increases it decreases (Fig. 20). Also wave period is effective on this parameter (Fig. 20). This dependence may be due to the diffraction around the piles as it changes the wave length. Yet, a certain judgement cannot be made regarding the 'wave height-wave transmission' relationship. As such, a dependence was not seen between those two parameters. Considering the tested waves, the transmission coefficients can be said to be in the range of 0.30–0.75. The velocity measurement results support this conclusion as well.

4. Conclusion

A model application of a piled wavescreen was performed in the laboratory conditions in this study. Dynamic pressures on the piles (along and around), water particle velocities at landward and seaward of the wavescreen and wave measurements were undertaken for a given structural configuration. Based on the experimental findings the following conclusions can be drawn.

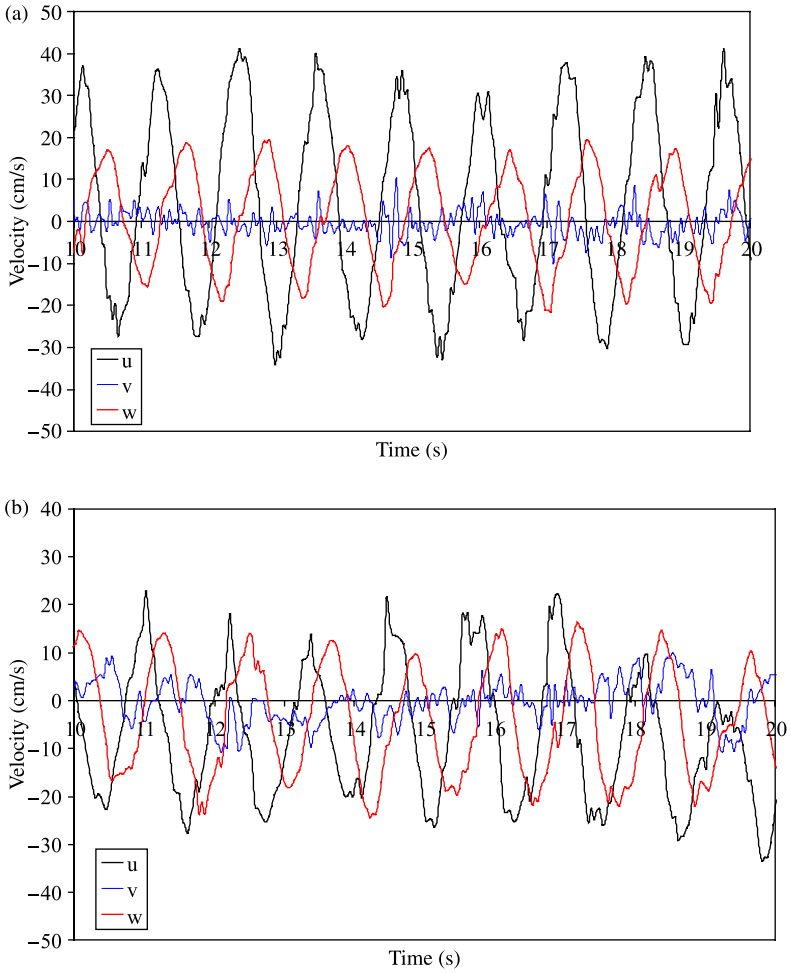

Fig. 18. The *u, v* and, *w* components of the water particle velocities recorded at the 0.45 m distance from the bottom for SWL = 0.65 m (a) at seaward of the wavescreen, (b) at landward of the wavescreen.

One of the main conclusions of pressure measurements was the exponentially decaying magnitude of dynamic wave pressures. As can be seen from the results presented in Section 3.1, there is a strong correlation between the 'pressure vs. depth' curves and logarithmic best fitting curves, both for regular and irregular waves. This correlation weakens as it approaches the still water level due to the nature of logarithmic functions as explained in the relevant section. This characteristic seemed not to be less dominant between the 'dimensionless pressure (P_d/P_d^*) vs. dimensionless depth (d/d^*)'.

Also the introduction of wave height and wave period to the dimensionless depth parameter, as denominator, seemed to reduce the scattering of the data. In other words, it maintained the gathering of the data within a relatively smaller range. This effect is more dominant with the wave period.

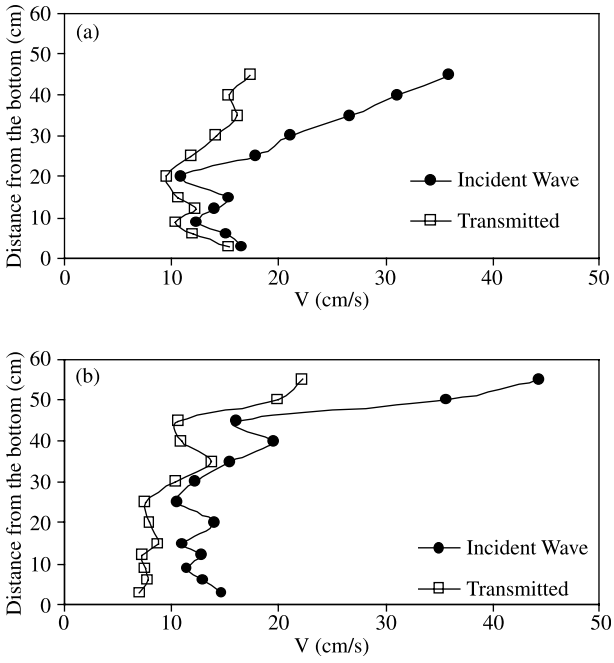

Fig. 19. The variation of velocity profiles with depth (a) for SWL=0.65 m, (b) for SWL=0.75 m.

The dynamic wave pressure measurements carried out around the piles with 22.5° intervals showed that the maximum dynamic wave pressure may not always be seen at the elementary surface normal to the wave direction. Findings show that the maximum dynamic wave pressure around the pile is closer to a location making an angle of 22.5° with the incident wave direction for 0.65 SWL. Normally, for a single pile the maximum

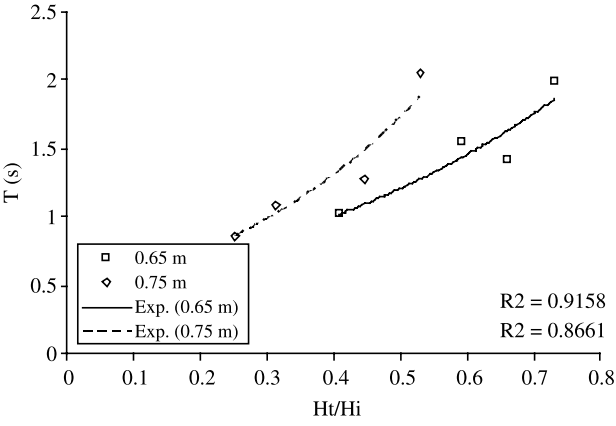

Fig. 20. Wave transmission coefficients vs. wave period for different water levels.

dynamic wave pressure is expected to occur at the infinitesimal area normal to wave. Such a switch of the location of maximum wave pressure may be explained due to the multi-cylinder effect and related to the pile spacing, pile diameter and wavelength parameters. This phenomenon should be further investigated in future studies.

Another surprising outcome of the pressure measurements was the variation of in-line components of dynamic wave pressures as this variation fits a third degree polynomial curve with a very high correlation. This dependency is also worth investigating in a further experimental study.

The vertical distribution of in-line dynamic wave force, which was calculated by summing the in-line components of dynamic wave pressures around the piles, also exhibits an exponentially decaying nature similar to the in-line dynamic wave pressures. As seen in in-line dynamic wave pressures, this characteristic becomes more significant with increasing depth. This can also be explained by the nature of logarithmic functions.

Water particle velocity measurements showed that horizontal velocity component 'u' is affected more drastically compared to vertical velocity component 'w' by the presence of the wavescreen. Also the data demonstrated that a lateral momentum transfer occurs at the landward of the wavescreen which indicates minor energy dissipation.

Furthermore, the pointwise velocity measurements were conducted using ADV and the velocity profiles were obtained at landward and seaward of the wavescreen for two different depths. These data indicated that within the region closer to the surface, the wavescreen has greater impact in terms of wave energy dissipation. In the region closer to the bottom, velocity values at the seaward and landward are quite close to each other. As a result, a considerable amount of wave energy is dissipated within the region close to the surface. This result is important since in a way it shows the wavescreen does not have significant influence in sediment transport phenomenon in spite of the fact that it dissipates wave energy efficiently. At this juncture, it can be concluded that wavescreen keeps the long-term coastal balance better than rubble mound breakwaters. This makes the wavescreen an environmentally friendly structure.

It should be borne in mind that the results in this study are obtained for the given structural configuration. Considering physical parameters (i.e. construction depth, d; pile diameter, D; spacing between the piles, S; vertical inclination angle, α; freeboard, f; wave length, L; etc.), the matter should be further investigated using various combinations of these. The authors hope that the results presented in this study are useful for the practitioners and helpful in their applications.

References

Akyildiz, A., 2002. Experimental investigation of pressure distribution on a cylinder due to the wave diffraction in a finite water depth. Ocean Engineering 29 (9), 1119–1132.

Anandkumar, G., Sundar, V., Graw, K.U., Kaldenhoff, H., 1995. Pressure and forces on inclined cylinders due to regular waves. Ocean Engineering 22 (7), 747–759.

Chakrabarti, S.K., 1978. Wave forces on multiple vertical cylinders. Journal of the Waterway, Port, Coastal and Ocean Division, ASCE 104 (WW2), 147–161.

Chakrabarti, S.K., 1981. Hydrodynamic coefficients for a vertical tube in an array. Applied Ocean Research 3 (1), 2–12.

Chakrabarti, S.K., 1982. Wave force coefficients for rough vertical cylinders. Journal of the Waterway, Port, Coastal and Ocean Division, ASCE 108 (4), 445–455.

Chakrabarti, S.K., Cotter, D.C., Libby, A.R., 1983. Hydrodynamic coefficients of a harmonically oscillated tower. Applied Ocean Research 5 (4).

Chan, E.S., Cheong, H.F., Tan, B.C., 1995. Laboratory study of plunging wave impacts on vertical cylinders. Coastal Engineering 25 (1–2), 87–107.

Cotter, D.C., Chakrabarti, S.K., 1984. Wave force tests on vertical and inclined cylinders. Journal of the Waterway, Port, Coastal and Ocean Division, ASCE 110 (1), 1–14.

Dean, R.G., Dalrymple, R.A., 1991. Water Wave Mechanics for Engineers and Scientists. World Scientific, Singapore, 353 pp.

Garrison, C.J., Field, J.B., May, M.D., 1977. Drag and inertia forces on a cylinder in periodic flow. Journal of Waterway, Port, Coastal and Ocean Engineering, ASCE 103 (2), 193–204.

Goda, Y., 1985. Random Seas and Design of Maritime Structures. University of Tokyo Press, 323 pp.

Morison, J.R., O'Brien, M.P., Johnson, J.W., Schaaf, S.A., 1950. The forces exerted by surface waves on piles. Petroleum Transactions, AIME (American Inst. Mining Eng.) 189, 149–154.

Sarpkaya, T., 1976. In-line and transverse forces on cylinders in oscillating flow at high reynolds number. Proceedings of Eighth A. Offshore Technological Conference, Houston, USA, pp. 95–108.

Sarpkaya, T., 1979. Hydrodynamic forces on various multiple tube riser configurations. Proceedings of Eleventh A. Offshore Technological Conference, Houstan, USA, pp.1603–1609.

Sumer, B.M., Fredsoe, J.E., 1997. Hydrodynamics around cylindrical structures., Advanced Series on Ocean Engineering World Scientific, Singapore pp. 273.

Sundar, V., Vengatesan, V., Anandkumar, G., Schlenkhoff, A., 1998. Hydrodynamic coefficients for inclined cylinders. Ocean Engineering 25 (4–5), 277–294.

Sundar, V., Koola, P.M., Schlenkhoff, A.U., 1999. Dynamic pressure on inclined cylinders due to freak waves. Ocean Engineering 26 (9), 841–863.

Yagci, O., Kapdasli, S., Cigizoglu, S., 2004. The stability of the antifer units used on breakwaters in case of irregular placement. Ocean Engineering 31 (8–9), 1111–1127.